Electrochemical and Solid-State Letters, **2** (9) 452-454 (1999)
S1099-0062(99)04-102-4 CCC: $7.00

Effect of Surface Modification on Catalytic Properties of $Sr_{0.25}Bi_{0.5}FeO_{3-\delta}$ Membranes

Xinyu Lu* **and Meilin Liu****,z**

School of Materials Science and Engineering, Georgia Institute of Technology, Atlanta, Georgia 30332-0245, USA

Membranes of mixed ionic-electronic conductors have been widely studied for gas separation, electrosynthesis, and removal of pollutants. Not only the rates but also the selectivities of these processes are determined critically by the surface catalytic properties of the membranes, which in turn are determined by the morphology, microstructure, and composition of the surfaces. In this study, nanoporous $Sr_{0.25}Bi_{0.5}FeO_{3-\delta}$ (SBF) layers, with or without the impregnation of catalysts, were applied to dense SBF membranes using a sol-gel process to investigate the effect of surface modification on the catalytic properties. It is found that both oxygen permeation rates and methane conversion of a dense SBF mixed-conducting membrane coated with a nanoporous SBF layer are much higher than those of an as-sintered SBF membrane without surface modification. Nanoparticles of nickel loaded into the porous SBF surface layer further enhanced methane conversion.

Manuscript submitted April 26, 1999; revised manuscript received June 1, 1999. Available electronically June 24, 1999.

Direct conversion of methane to syngas (*i.e.*, CO and H_2) or high-value hydrocarbons has been investigated through partial electrochemical oxidation of methane using ionic conductors such as yttria-stabilized zirconia (YSZ)[1-5] or ytterbia-doped strontium cerate[6,7] with a configuration similar to that of a solid oxide fuel cell. The electrochemical cell delivers oxygen from air to the sites for partial oxidation of methane with oxygen ions (O^{2-}) or atomic oxygen (O), which are believed to be more catalytically active than molecular oxygen (O_2) for partial oxidation of methane. The use of a mixed ionic-electronic conductor (MIEC) membrane, however, has attracted much attention because of the simplicity in construction and operation of a membrane reactor system. In fact, a dense MIEC membrane, when used for methane conversion, delivers pure oxygen from air to the methane feed stream, driven by the gradient in the partial pressure of oxygen across the membrane. The flux of oxygen-related defects (oxygen vacancies or interstitials) is counterbalanced by a flux of electrons (e^-) or electron holes ($h^\bullet$). Indeed, a MIEC membrane alone has a function similar to that of an electrochemical cell for methane conversion. In particular, the membrane can be fabricated readily in a thin-film form (supported by a porous substrate) to enhance significantly the rate of methane conversion, as demonstrated in oxygen separation using thin-film membranes of Bi_2O_3-based mixed conductors[8] and perovskite-type MIECs such as $SrCo_{0.8}Fe_{0.2}O_{3-\delta}$.[9,10]

MIECs can be used not only as membrane but also as electrodes or catalysts in solid-state ionic devices due to their inherent catalytic activity.[11-13] It is well recognized that the number of active sites for electrochemical reactions may be increased dramatically, from triple-phase boundaries at electrolyte-electrode interfaces for an electrode of a pure electronic conductor to the entire MIEC/gas interfaces for an electrode of a MIEC.[14,15] For solid-state electrochemical systems based on thin-film ceramic membranes such as a MIEC membrane for methane conversion or a solid oxide fuel cell (SOFC), the rate of the overall process or the efficiency of the system depends sensitively on the interfacial resistance, which becomes more significant as the membrane thickness or the operating temperature is reduced. For methane conversion, in particular, the surface catalytic properties of a membrane determine not only the rate of methane conversion but also the products to which the methane is converted.

Recent studies indicate that $Sr_{0.25}Bi_{0.5}FeO_{3-\delta}$ (SBF) has great potential for methane conversion; SBF membranes display high oxygen permeation rates, remarkable stability under conditions for methane conversion[16] and a much lower coefficient of thermal expansion than cobalt-containing MIECs such as $La_{1-x}Sr_xCoO_{3-\delta}$ and $La_{1-x}Sr_xCo_{1-y}FeyO_{3-\delta}$.[17] In this study, the surface morphology, microstructure, and composition of a dense SBF membrane are modified, and the effect of surface properties on the oxygen separation rates and methane conversion of SBF membranes is characterized.

Experimental

A conventional ceramic process was used to prepare dense (SBF) membranes. Precursors for SBF were $SrCO_3$ (98+%), Bi_2O_3 (99.9%), and Fe_2O_3 (99+%), all from Aldrich Chemical Company. Stoichiometric amounts of precursors were ballmilled in ethanol for 24 h, then calcined in air at 800°C for 10 h to form a crystalline phase of SBF.[17] The calcined powders were examined using X-ray diffraction (XRD, Philips, PW1800 with Cu Kα radiation) to determine the phase composition. In case of incomplete calcination, ballmilling and calcination were repeated until a pure phase was obtained. The powder with desired phase was then pressed into pellets (20 mm diam) and subsequently sintered in air at 1000°C for 5 h to achieve sintered densities greater than 95% of the theoretical values.

Porous SBF films.—The SBF powder and a binder (V-006, Heraeus) were blended to form a slurry, which was then brush-painted on dense SBF pellets and subsequently fired at 800°C for 30 min to form a porous SBF layer (about 6 μm thick) on both sides of a dense SBF pellet.

Nanoporous SBF films.—Stoichiometric amounts of $Sr(NO_3)_2$, $Bi(OOCCH_3)_3$, and $Fe(NO_3)_3 \bullet 9H_2O$ were added to deionized water at 60°C under vigorous stirring, and nitric acid was gradually added to the solution until the $Bi(OOCCH_3)_3$ was completely dissolved. Then, citric acid was added to the solution. The molar ratio of citric acid to metal ion was 1.5~2 to 1. The pH of the solution was adjusted to ~5-6 by gradual addition of NH_4OH under stirring before the solvent was slowly evaporated to form a homogeneous and viscous sol. The sol was coated onto the dense SBF membranes using a spin coater. After drying at about 100°C for 2 h, the coated pellets were fired at 750°C for 30 min. The thicknesses of the sol-gel derived coatings were about 0.2 μm. Nickel catalyst was prepared by impregnation of an aqueous solution of $Ni(NO_3)_2 \bullet 6H_2O$ (Aldrich) into the nanoporous SBF films. After drying at 80°C for 24 h and firing in air at 600°C for 2 h, the film was exposed to a 5% H_2/Ar stream at 500°C for 1 h to form nanoparticles of nickel metal in the nanoporous SBF layer. The surface microstructures of dense SBF membranes with and without surface modification were examined using a scanning electron microscope (SEM, Hitachi S800) and a transmission electron microscope (TEM, Hitachi HF2000).

The arrangement for oxygen permeation and methane conversion measurements was as described elsewhere in Ref. 16. The SBF pellet (0.55 mm thick and 17 mm in diam) was sealed to the top of an alumina tube using a homemade glass. For direct comparison, oxygen permeation rates were measured at a constant flow rate of carrier gas (15 mL/min), which was blown from the central tube toward

* Electrochemical Society Student Member.
** Electrochemical Society Active Member.
z E-mail: meilin.liu@mse.gatech.edu

S1099-0062(99)04-102-4 CCC: $7.00

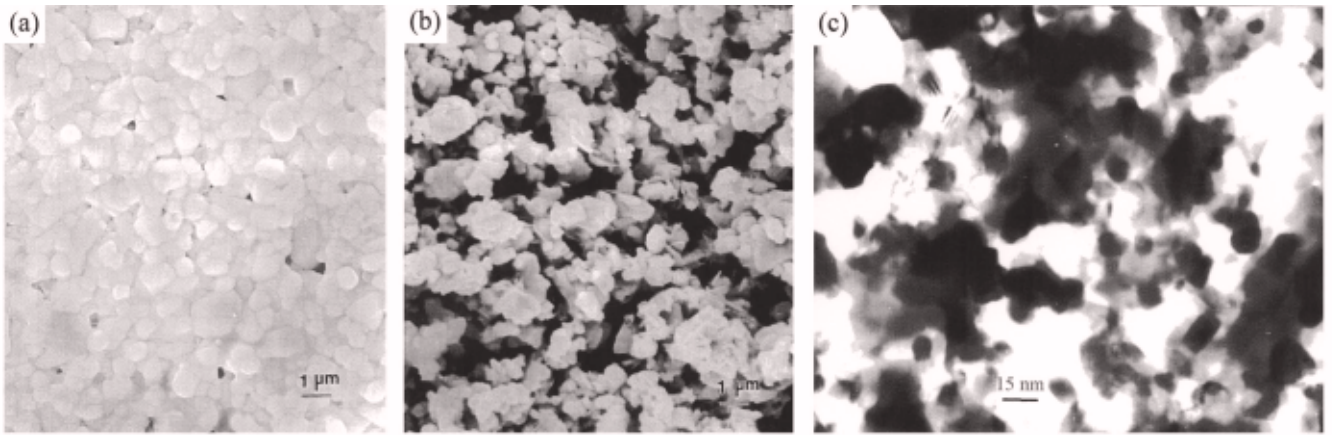

Figure 1. The surface morphologies of (a) a dense as-sintered SBF membrane, (b) a porous SBF layer (brush-painted) coated on a dense SBF membrane, and (c) a nanoporous SBF layer (sol-gel derived) coated on a dense SBF membrane.

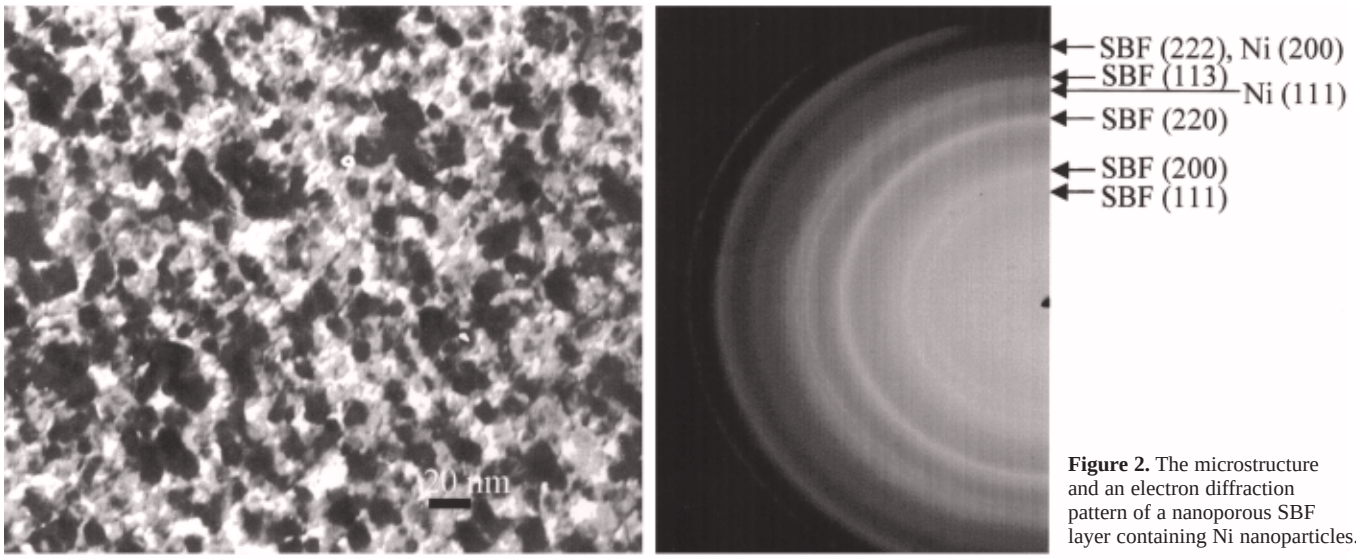

Figure 2. The microstructure and an electron diffraction pattern of a nanoporous SBF layer containing Ni nanoparticles.

the membrane surface. The clearance between the end of the central tube (5 mm i.d. and 6.5 mm o.d.) in the reactor and the membrane surface was less than 5 mm. It was critical to keep this clearance as small as possible to reduce the dead volume. One side of the membrane was exposed to air while the other side was exposed either to pure argon to measure oxygen permeation rates or to diluted methane to measure methane conversion. Two mass flow controllers (Omega FMA760 series) were used to maintain stable and constant gas flows. The inlet methane concentration and the outgoing product gases were analyzed using an online gas chromatograph (GC, Varian 3800), which was equipped with two detectors, a thermal conductivity detector (TCD) and a flame ionization detector (FID). The elemental gases were detected by TCD using argon as carrier gas. This provided the best detection of hydrogen while still providing adequate detection of oxygen and nitrogen. FID was used to detect hydrocarbons and carbon oxides, which were converted to methane by means of a nickel catalyst or methanizer. A serial/bypass configuration was arranged for two isothermal columns (40°C), a molecular sieve 13X (45/60) for the lighter gases and a porous polymer Hayesep N (80/100) for the heavier gases (CO_2 and C_2 hydrocarbons). Two automatic switching valves, an 8-port valve (V1) and a 10-port valve (V2), were connected to the columns so that the position of the valve selected which column was directed to the detector and, in turn, which column was backflushed to vent. H_2, O_2, N_2, CH_4, and CO were eluted earlier than CO_2 and the C_2 hydrocarbons in a molecular sieve 13X column and passed to the TCD. After the CO eluted, V1 was switched to direct the porous polymer effluent to the FID for measurement of CO_2 and C_2 hydrocarbons. Multiple-point calibration curves for the glassy carbon (GC) were created and recalibrated periodically for long-term measurements. The separation of the O_2 peak from the N_2 peak was important in order to detect leaks through the membrane or the glass sealing. An N_2 peak would be detected using the GC if air leaked through the membrane or glass sealing. The methane conversion was estimated from

$$CH_4 \text{ conversion } \% = [(F_{Ch4,inlet} - F_{CH4,outlet})/F_{CH4,inlet}] \times 100\% \quad [1]$$

Results and Discussion

Shown in Fig. 1 are the surface views of a dense as-sintered SBF membrane, a porous SBF layer coated on a dense SBF membrane, and a nanoporous SBF layer (derived from the sol-gel process) coated on a dense SBF membrane. The surface of the as-sintered SBF (Fig. 1a) is relatively dense and the average grain size is about 1 μm. The porous SBF coating (Fig. 1b) has large pores, but the grain size is also about 1 μm. The nanoporous SBF coating (Fig. 1c) derived from the sol-gel process consists of much finer grains (~10-20 nm), offering much more surface areas for gas adsorption-desorption and catalytic reactions. Figure 2 shows the microstructure and an electron diffraction pattern of a nanoporous SBF coating containing about 30 wt % nanoparticles of nickel, as determined using energy dispersive spectroscopy on a TEM. It appears that the nanoporous structure of SBF prevented the nickel particles from agglomeration. The size of nickel particles varied from 10 to 20 nm and they were uniformly dispersed in the nanoporous SBF layer. Because the d-

S1099-0062(99)04-102-4 CCC: $7.00

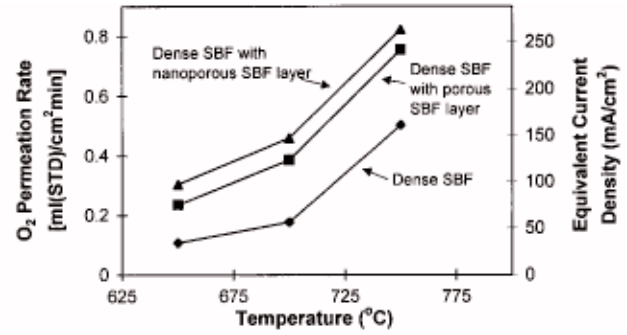

Figure 3. Oxygen permeation rates of dense SBF membranes with or without surface modification, as measured in an oxygen concentration cell of Ar | SBF membrane | air.

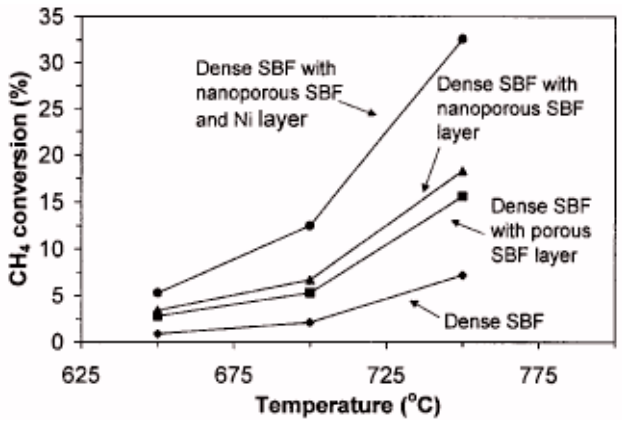

Figure 4. Methane conversion of dense SBF membranes with or without surface modification, as measured in a reactor of (CH_4 + Ar) | SBF membrane | air.

spacing of Ni(111) is too close to that of SBF(113). It was difficult to obtain a dark-field image of Ni to show the distribution of Ni particles in the composite.

Figure 3 shows oxygen permeation rates, measured at temperatures from 650 to 750°C, of SBF membranes (0.55 mm thick) with or without surface modification. The effect of surface modification on rates of oxygen permeation is clear. In terms of current density due to the motion of oxygen-related defects through the membrane, the oxygen permeation rates at 750°C varied from about 150 mA/cm^2 for the membrane without surface modification, to about 225 mA/cm^2 when coated with a porous SBF layer (brush printed), and to about 240 mA/cm^2 when coated with a nanoporous layer of SBF (sol-gel derived). The activation energy for oxygen permeation, as estimated from the slopes of the Arrhenius plots (log J_{O2} *vs.* 1/*T*), varied from (120 ± 29) kJ/mol for the dense SBF membrane without surface modification, to (91 ± 11) kJ/mol for the membrane coated with a coarse porous SBF layer, and to (78 ± 10) kJ/mol for the membrane coated with a nanoporous SBF layer. The lower the activation energy, the higher the oxygen permeation rate. It is further anticipated that as the thicknesses of the SBF membranes are reduced, the effect of surface modifications on the rates of oxygen separation will be even more dramatic. Additionally, because the thermal expansion coefficients of SBF are similar to that of YSZ, porous SBF may be a good cathode material for YSZ-based intermediate-temperature SOFCs.

Figure 4 shows methane conversion of the membranes (0.55 mm thick) with or without surface modification at different temperatures. Again, the effect of surface modification on methane conversion is significant. At 750°C, the methane conversion varied from about 7% for the membrane without surface modification, to 15% for the membrane with a coarse porous surface layer, and to 18% for the membrane with a nanoporous surface layer. Further, the membrane coated with a layer of a nanocomposite of SBF and Ni exhibited the highest methane conversion (~32%), clearly implying that Ni has catalytic effect for methane conversion. In the last case, it is noted that methane was converted primarily to H_2 and CO (selectivity, 95%) with small amounts of CO_2 and H_2O. In the case without Ni catalyst, however, the methane conversion products were predominantly CO_2 (80%) and C_{2+} (20%), implying that SBF promotes complete, rather than partial, oxidation of methane. Although it is apparent that the observed dramatic effect is due at least in part to the surface area or the number of reaction sites at the MIEC/gas interface, it is not clear, however, how other microscopic features may influence the catalytic properties of the surfaces.

Conclusions

Nanoporous SBF layers with and without a nickel catalyst have been applied to $Sr_{0.25}Bi_{0.5}FeO_{3-\delta}$ membranes using a sol-gel process to attain large surface areas. Surface modifications have dramatic effects on surface catalytic properties of SBF dense membranes. Oxygen permeation rates and methane conversion of a dense SBF membrane coated with a nanoporous SBF thin layer are much higher than those of a bare SBF membrane. A nickel catalyst dispersed into a nanoporous SBF layer, forming a nanocomposite of SBF and Ni, further enhanced methane conversion. Although the influence of surface microstructure and composition on oxygen permeation and methane conversion is clear and dramatic, the effect of surface microscopic features on the pathways and mechanisms of interfacial reactions remains under investigation. Detailed mechanistic studies of oxygen reduction and evolution and methane conversion on these surfaces will be discussed in subsequent communications.

Acknowledgment

This work was supported by National Science Foundation under grant no. CTS-9705541. The assistance of Jinsong Yin and Yongqian Wang in TEM analysis is gratefully acknowledged.

The Georgia Institute of Technology assisted in meeting the publication costs of this article.

References

1. K. Otsuka, K. Suga, and I. Yamanaka, *Chem. Lett.*, 317 (1988).
2. K. Otsuka, K. Suga, and I. Yamanaka, *Catal. Lett.*, **1**, 423 (1988).
3. N. U. Pujare and A. Sammells, *J. Electrochem. Soc.*, **135**, 2544 (1988).
4. B. C. H. Steele, I. Kelly, H. Middleton, and R. Rudkin, *Solid State Ionics*, **28-30**, 1547 (1988).
5. D. Eng and M. Stoukides, *Catal. Lett.*, **9**, 47 (1991).
6. H. Iwahara, H. Uchida, K. Morimoto, and S. Hosogi, *J. Appl. Electrochem.*, **19**, 448 (1989).
7. P. H. chiang, D. Eng., and M. Stoukides, *J. Electrochem. Soc.*, **138**, L11 (1991).
8. M. Liu, Y. Shen, A. Joshi, and K. Krist, U.S. Pat. 5,273,628 (1993).
9. T. H. Lee, Y. L. Yang, A. J. Jacobson, B. Abeles, and M. Zhou, *Solid State Ionics*, **100**, 77 (1997).
10. T. H. Lee, Y. L. Yang, A. J. Jacobson, B. Abeles, and S. Milner, *Solid State Ionics*, **100**, 87 (1997).
11. H. Anderson, *Solid State Ionics*, **52**, 33 (1992).
12. W. Worrell, W. Weppner, and H. Schubert, U.S. Pat. 4,931,214 (1990).
13. H. Tuller and P. Moon, *Mater. Sci. Eng., B*, **1**, 171 (1988).
14. M. Liu, *J. Electrochem. Soc.*, **145**, 142 (1998).
15. M. Liu and J. Winnick, *Solid State Ionics*, **118**, 11 (1999).
16. X. Lu and M. Liu, in *Solid-State Ionic Devices*, E. D. Wachsman, M. Liu, J. R. Akridge, and N. Yamazoe, Editors, PV 99-13, The Electrochemical Society Proceedings Series, Pennington, NJ (1999), In press.
17. L. Siwen, Y. Weishen, F. Liangqing, and L. Liwu, *J. Solid State Chem.*, **130**, 316 (1997).